Electronic Supplementary Material (ESI) for Chemical Communications.
This journal is © The Royal Society of Chemistry 2019

Electronic supplementary information

Electrocatalysis of S-doped carbon with weak polysulfide adsorption enhances lithium-sulfur batteries performance

Lingyu Du, Xueyi Cheng, Fujie Gao, Youbin Li, Yongfeng Bu, Zhiqi Zhang, Qiang Wu, Lijun Yang, Xizhang Wang, Zheng Hu**

Key Laboratory of Mesoscopic Chemistry of MOE and Jiangsu Provincial Laboratory for Nanotechnology, School of Chemistry and Chemical Engineering, Nanjing University, Nanjing 210023, China.

* Corresponding Authors. E-mail: wqchem@nju.edu.cn (Q. Wu); zhenghu@nju.edu.cn (Z. Hu)

1. Experimental Section

1.1 Materials preparation

Hierarchical S-doped carbon nanocages (hSCNC) were prepared by in situ MgO template method with thiophene precursor, which possessed the S content of 3.1 at.% (Table S1).[1] The hCNC without S doping was also prepared with benzene precursor for comparison.[2]

The sulfur was filled into hSCNC or hCNC via a melt-infusion process, similar to our previous study.[3] The sulfur and hSCNC or hCNC mixture was obtained by the disproportionation reaction of $Na_2S_2O_3$ in the acid suspension followed by washing and drying. Afterwards, the mixtures were heated at 155 °C for 12 h under Ar protection to infiltrate sulfur into the nanocages, and further heated at 250 °C for 1.5 h to evaporate sulfur outside the nanocages. The corresponding composites were denoted as S@hSCNC and S@hCNC, respectively.

1.2 Material characterizations

Scanning electron microscopy (SEM, Hitachi S4800 at 5 kV), high resolution transmission electron microscopy (HRTEM, JEM-2100), X-ray diffraction (XRD, Bruker X-ray diffractometer, D8 Advance A25, Co target, $\lambda_{K\alpha1}$ = 0.178897 nm) and X-ray photoelectron spectroscopy (XPS, PHI 5000 Versa Probe) were used to characterize the morphologies, structures, and compositions of the samples. The scanning transmission electron microscopy (STEM) and elemental mapping images were obtained on JEM-2100F. N_2 adsorption-desorption isotherms were obtained on Thermo Fisher Scientific Surfer Gas Adsorption Porosimeter at 77 K. The specific surface area was calculated using the Brunauer-Emmett-Teller (BET) method based on the adsorption data in the linear relative pressure (p/p_0) range of 0.05–0.35. The pore size distribution was calculated from the corresponding adsorption branch of N_2 isotherm by Horvath-Kawazoe method for micropore and Barrett-Joyner-Halenda method for mesopore. The sulfur contents in the S@hSCNC and S@hCNC composites were measured by thermogravimetry analysis (Netzsch STA-449F3), which was performed from room temperature to 600 °C at a heating rate of 10 °C min^{-1} under Ar. The conductivity was measured by a four-probe method using a source measure unit (Keithley 6430). UV-vis adsorption spectra were measured using a Shimadzu UV-2600 spectrophotometer.

1.3 Battery assembly and electrochemical tests

The Li-S batteries were assembled in an Ar-filled glove box with lithium metal plate as anode. A homogeneous slurry was made by mixing 80 wt% S@hSCNC (or S@hCNC) composite, 10 wt% acetylene black and 10 wt% polyvinylidene fluoride in N-methyl-2-pyrrolidinone. The sulfur cathodes were prepared by spreading the slurry on the carbon-coated aluminum foil and drying at 70 °C for 12 h. In the normal measurements, the areal sulfur loading was 0.8–1.1 mg cm^{-2}, the electrolyte was 40 μL of 1.0 mol L^{-1} LiTFSI dissolved in a mixture of 1,3-dioxolane (DOL) and 1,2-dimethoxyethane (DME) (1:1 v/v) with lithium nitrate (2 wt%) as additive, and the separator

was polypropylene membrane (Celgard 2500).

In order to achieve high areal capacity, the Li-S battery was constructed by the cathode with high sulfur loading of 4.5–5.0 mg cm^{-2}, the Li plate anode and the separator of carbon-based nanocages-coated Celgard 2500 (Fig. S9) [3] with the electrolyte/sulfur (E/S; μL_E mg^{-1}_S) ratio of 15.

The electrochemical tests were performed on a Lanhe CT2001A battery tester in the potential window of 1.7–2.8 V. Before cycling tests at 2 A g^{-1}, 5 cycles at a low current density of 0.1 A g^{-1} were performed to activate the electrode. Cyclic voltammetry (CV) was measured at a scan rate of 0.1 mV s^{-1} within 1.7–2.8 V on VMP3 electrochemical workstation (Bio-logic).

1.4 Theoretical calculations

The spin-unrestricted density functional theory (DFT) calculations were carried out by the Dmol3 code from Accelrys.[4, 5] The generalized gradient-corrected Perdew-Burke-Ernzerhof (PBE/GGA) function,[6] along with a double numerical basis set including p-polarization function (DNP), was applied to the geometry optimization and vibrational analysis. Dispersion-corrected DFT (DFT-D) scheme was used to describe the van der Waals (vdW) interaction. During the coordinates relaxation, the tolerances of energy and force were 1×10^{-5} Ha and 0.002 Ha $Å^{-1}$, and the maximum displacement was 5×10^{-3} Å, respectively. The Monkhorst-Pack k-point mesh was 4×4×1 for the graphite plane model and 4×1×1 for thiophenic S-doped graphite plane model. The global orbital cutoff was 5.1 Å in all calculations.

For a quantitatively description of the interactions between the carbon and the S-containing clusters, the binding energy E_b was defined as follows.

$E_b = (E_{carbon} + E_S) - E_{total}$

Where E_{carbon}, E_S, and E_{total} represent the total energies of the carbon, an isolated sulfur-containing cluster (Li_2S_4, Li_2S_6 and Li_2S_8), and a certain carbon binding to a sulfur-containing cluster, respectively. The higher absolute value of binding energy corresponds to the stronger interaction.

The detailed calculation method of free energy diagrams is similar to our previous study.[3]

2. Supplementary Figures and Tables

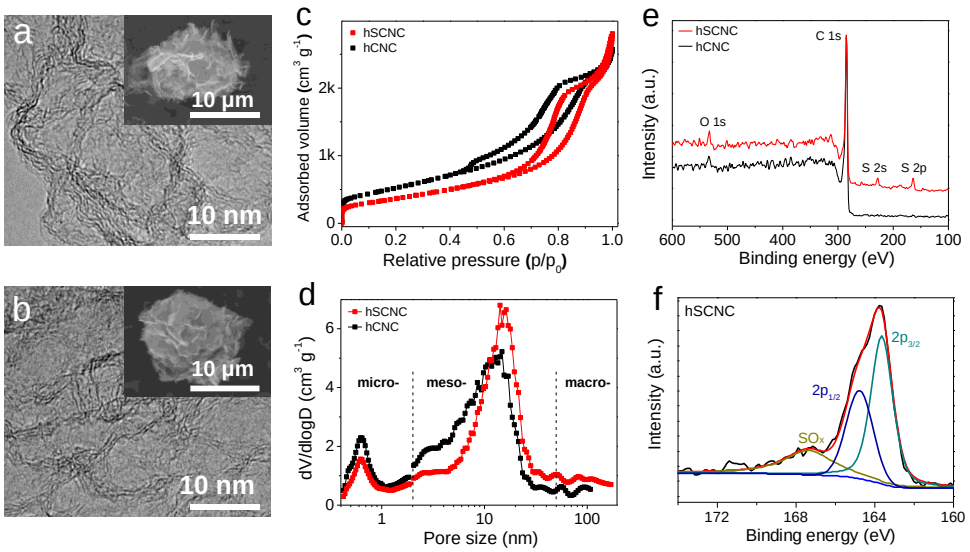

Fig. S1 Morphological, structural and component characterizations of the hSCNC and hCNC. (a,c) HRTEM images, insets show the SEM images. a) hSCNC, b) hCNC. (c,d) N_2 adsorption-desorption isotherms and corresponding pore size distributions. (e) XPS full spectra. (f) S 2p fine spectrum for hSCNC.

Table S1. The physical properties of hSCNC and hCNC.

	Specific surface area (m^2 g^{-1})	Mesopore volume (cm^3 g^{-1})	Micropore volume (cm^3 g^{-1})	Conductivity (S m^{-1})	Elemental content (at.%)		
					C	O	S
hCNC	1914	3.71	0.72	541	97.8	2.2	0
hSCNC	1296	3.91	0.51	138	94.2	2.7	3.1

Both hSCNC and hCNC are assembled by the micrometer-sized nanosheets with submicron interspace, and the nanosheets consist of the interconnected cuboidal hollow nanocages of 10–20 nm in size and shell thickness of 3–5 carbon layers (Fig. S1a,b). These nanocages possess large pore volumes, multi-scale pore structure and high conductivity (Fig. S1c,d, Table S1). The hSCNC sample consists of C, O and S elements with the S-doping content of 3.1 at.% (Fig. S1e). The S 2p fine spectrum can be deconvoluted into two kinds of sulfur species, i.e., the C–S–C moieties (79%) with spin split $2p_{1/2}$ and $2p_{3/2}$ [7] and the partially oxidized sulfur species SO_x (21%) [8] (Fig. S1f). This indicates that the sulfur dopants mainly exist as thiophenic-S species.

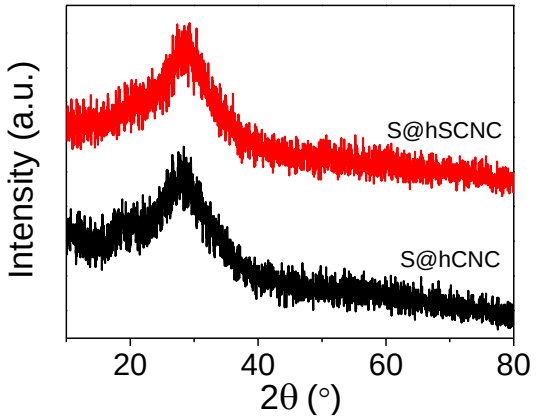

Fig. S2 XRD patterns of S@hSCNC and S@hCNC composites.

No diffraction peaks for sulfur were observed in the XRD patterns, indicating the sulfur infiltration into the carbon nancages with small grains.

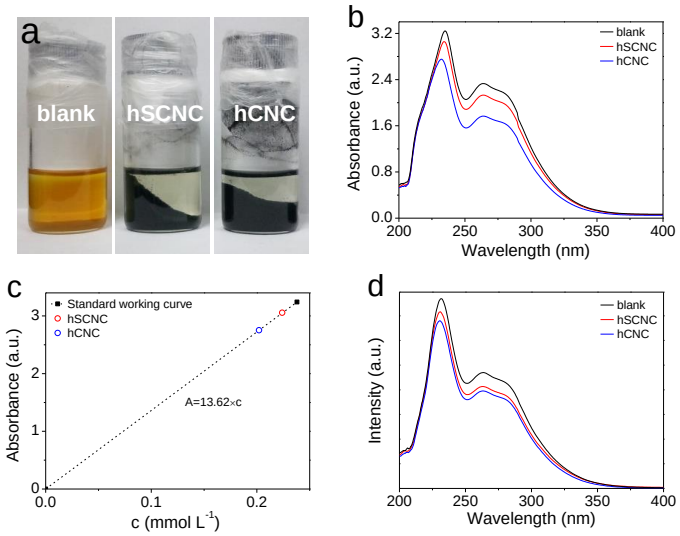

Fig. S3 (a) Photographs of the blank, hSCNC-soaked and hCNC-soaked Li_2S_6/DOL&DME solutions after 8 h soaking. (b) The UV-vis spectra of the corresponding Li_2S_6 solutions before and after soaking with hSCNC and hCNC with the same mass. (c) The standard absorbance-concentration curve based on the datum for the blank Li_2S_6 solution (■) and the zero-point. The red hollow circle (○) and blue hollow circle (○) correspond to the points of the Li_2S_6 solutions after hSCNC-soaking and hCNC-soaking, respectively. (d) The UV-vis spectra of the solutions before and after soaking with hSCNC and hCNC with the same surface area (~ 25.9 m^2). Note: Before the UV-vis measurements, 150 μL of the residual solution was diluted with 3 mL of DOL&DME solvent.

In the adsorption tests, Li_2S_6/DOL&DME solution (5.0 mmol L^{-1}) was prepared by mixing Li_2S and S with a desired ratio in anhydrous DOL and DME (1:1 v/v) at 50 °C in an Ar-filled glovebox. The blank solution is in orange. 20 mg of hSCNC or hCNC was dispersed into the solution (4 mL) to observe the color change with time. After 8 h soaking, both solutions after hSCNC and hCNC soaking became light yellow (Fig. S3a). The absorbance of the hSCNC-soaked solution was higher than that of the hCNC-soaked one, indicating the weaker LiPSs adsorption on the former (Fig. S3b). The absorbance of the residual solutions was normalized by the surface area of hSCNC and hCNC. According to the Lambert-Beer's law: $A = k \times c$ (here A is the absorbance of the solution, k the slope of the standard absorbance-concentration curve, c the amount of substance concentration of absorbent), the k value was roughly calculated to be 13.62 by plotting the datum for the blank solution and the zero-point (Fig. S3c). Then the residual concentrations of Li_2S_6 solution after soaking with hSCNC and hCNC can be determined. Thus the quantities of Li_2S_6 adsorbed on the surface of hSCNC and hCNC were calculated to be ~ 4.57×10^{-5} and 7.91×10^{-5} mmol m^{-2}, respectively. This indicates the weaker adsorption of Li_2S_6 on the former than on the latter.

In addition, the adsorption experiment was also performed by keeping the amount of hSCNC (20 mg) and decreasing the amount of hCNC to 13.5 mg with the same surface area of ~ 25.9 m^2. The UV-vis spectra of the blank, hSCNC-soaked and hCNC-soaked solutions were shown in Fig. S3d, which also indicates the larger absorbance thereof the weaker adsorption of Li_2S_6 on the hSCNC than on the hCNC, in accordance with the result in Fig. S3b.

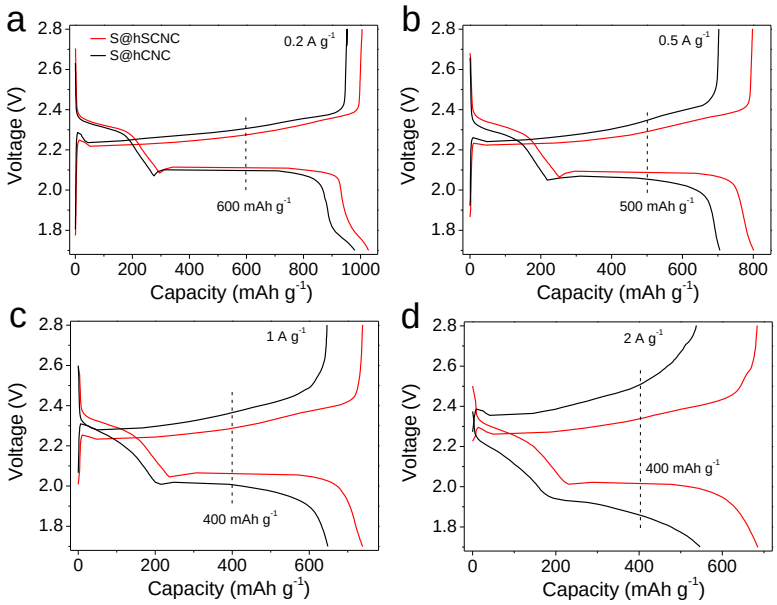

Fig. S4 Charge-discharge profiles for S@hSCNC and S@hCNC at different current densities. (a) 0.2 A g^{-1}. (b) 0.5 A g^{-1}. (c) 1 A g^{-1}. (d) 2 A g^{-1}.

Fig. 3b in the main text is obtained according to the charge-discharge profiles in Fig. S4. The potentials for S@hSCNC cathode are determined at the half specific capacities as marked, and those for S@hCNC cathode are read at the same capacities for better comparison. The potential gaps of S@hSCNC cathode are smaller than that of S@hCNC, indicating the smaller polarization effect for the former.

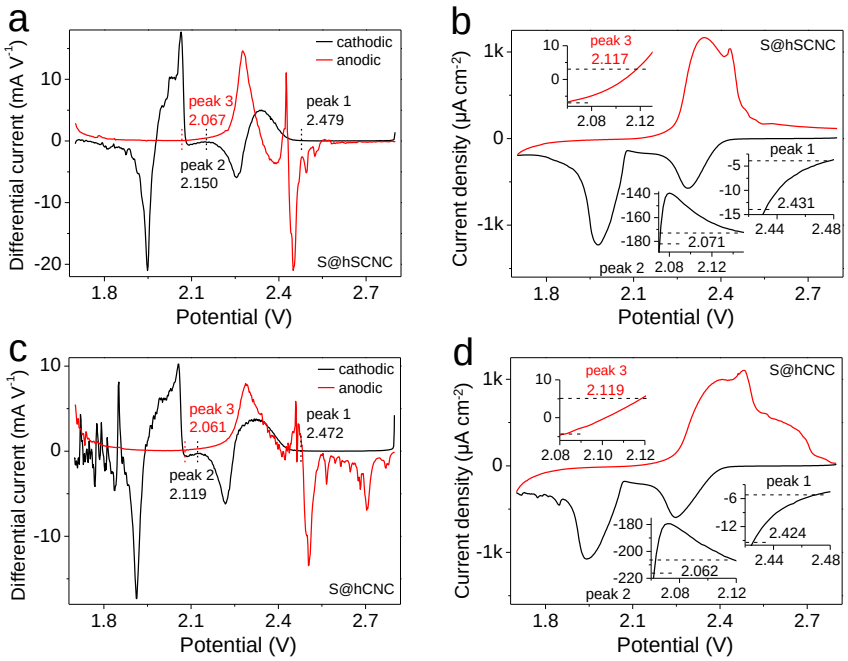

Fig. S5 Electrocatalytic effect of hSCNC on LiPSs conversion. (a,c) Differential CV curves, the baseline voltage is defined when the variation on current density is the smallest, i.e. dI/dV=0. (b,d) Corresponding onset potentials of redox peaks, the onset potential is determined when the current density goes 10 μA cm^{-2} beyond the corresponding current density at baseline.

The S@hSCNC cathode shows higher reduction and lower oxidation onset potentials than that of the S@hCNC, indicating the higher catalytic activity of the hSCNC.

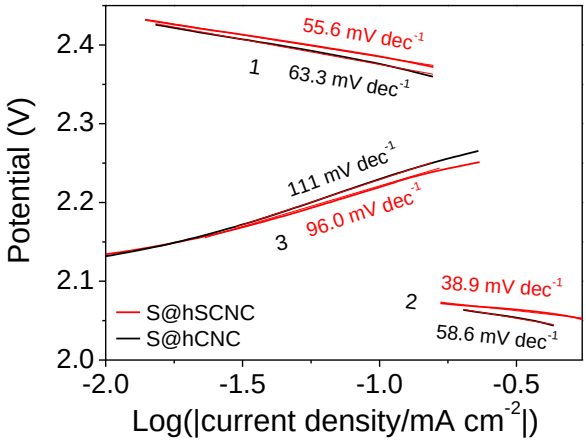

Fig. S6 Tafel plots for the redox reactions in S@hSCNC and S@hCNC batteries.

The Tafel slopes for the CV of S@hSCNC are smaller than that for the S@hCNC case, indicating the accelerated conversion kinetics for the former owing to the electrocatalysis promotion of S-doping.

Theoretical calculation: The reaction steps are described by equations S1~S6. The asterisk (*) indicates the species in adsorbed state.

$S_8 + 16\ Li^+ \rightarrow S_8^* + 16\ Li^+$ (S1)

$S_8^* + 16\ Li^+ + 2\ e^- \rightarrow Li_2S_8^* + 14\ Li^+$ (S2)

$Li_2S_8^* + 14\ Li^+ + 2\ e^- \rightarrow Li_2S_6^* + Li_2S_2 + 12\ Li^+$ (S3)

$Li_2S_6^* + Li_2S_2 + 12\ Li^+ + 2\ e^- \rightarrow Li_2S_4^* + 2\ Li_2S_2 + 10\ Li^+$ (S4)

$Li_2S_4^* + 2\ Li_2S_2 + 10\ Li^+ + 2\ e^- \rightarrow Li_2S_2^* + 3\ Li_2S_2 + 8\ Li^+$ (S5)

$Li_2S_2^* + 3\ Li_2S_2 + 8\ Li^+ + 8\ e^- \rightarrow Li_2S^* + 7\ Li_2S$ (S6)

Table S2. Free energies for each state (eV).

States	S_8	S_8*	Li_2S_8*	Li_2S_6*	Li_2S_4*	Li_2S_2*	Li_2S*
isolated	0	0	-1.58	-1.89	-1.75	-0.91	6.14
thiophenic S-doped graphite plane	0	-0.94	-2.99	-4.25	-5.35	-6.04	-3.20
graphite plane	0	-1.13	-3.33	-4.60	-5.43	-5.75	-2.01

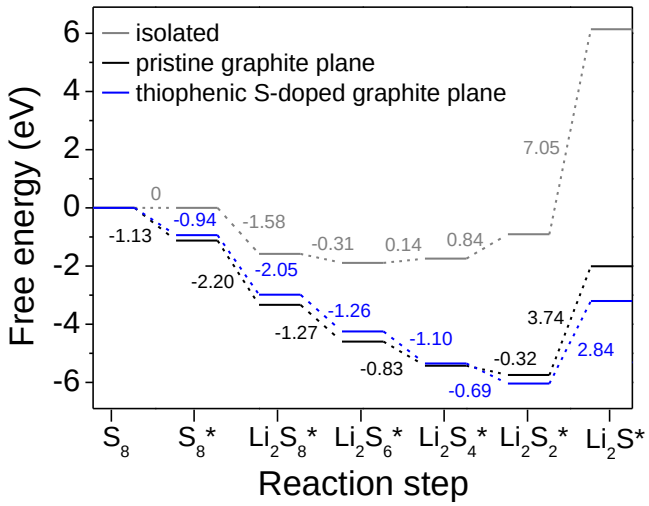

Fig. S7 Free energy diagrams of the discharge process on the thiophenic S-doped graphite plane and pristine graphite plane. The reaction steps include the adsorption of S_8 and its successive reductions to Li_2S_8, Li_2S_6, Li_2S_4, Li_2S_2 and Li_2S, respectively. The change value of the free energy for the two adjacent reaction steps was also indicated. For comparison, the process for the isolated case, i.e., without support, is also presented.

The sulfur reduction is more favorable on the thiophenic S-doped graphite plane than on the graphite plane, especially for the conversion from Li_2S_2 to Li_2S.

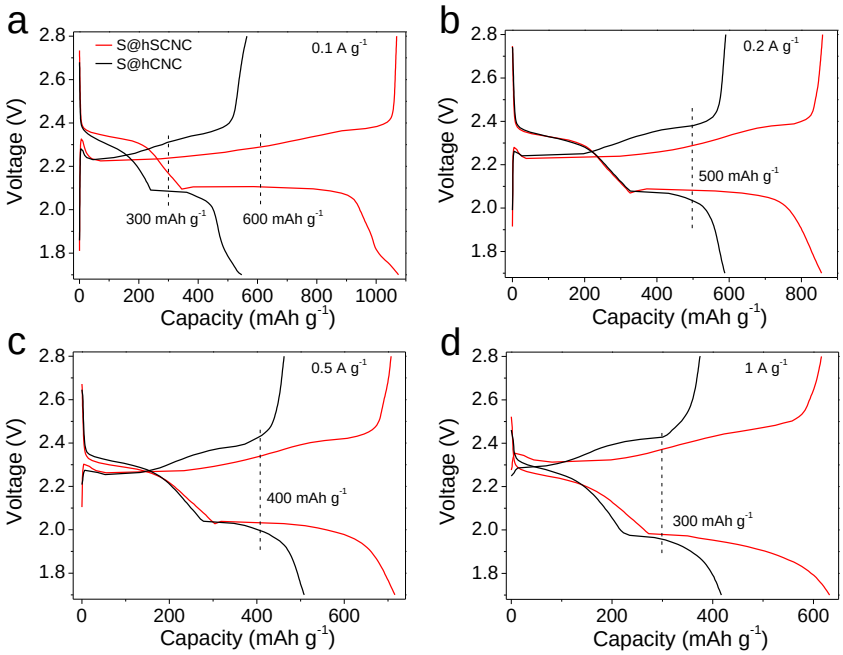

Fig. S8 Charge-discharge profiles of the Li-S batteries with high areal sulfur loading at different current densities. (a) 0.1 A g^{-1}. (b) 0.2 A g^{-1}. (c) 0.5 A g^{-1}. (d) 1 A g^{-1}.

S@hSCNC cathode presents smaller potential gaps than the undoped carbon counterpart, indicating the effectiveness of the S-doping carbon under high sulfur loading.

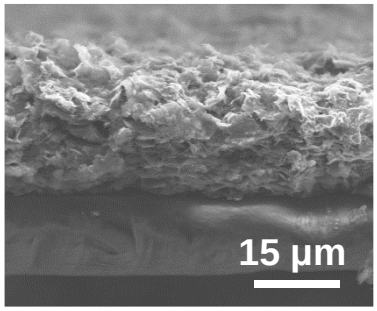

Fig. S9 SEM image of the hSCNC-modified Celgard 2500.

In the Li-S batteries with high-sulfur-loading cathode, the carbon-modified separators are used. The hSCNC (or hCNC) modified separator was obtained by coating the slurry of hSCNC (or hCNC) and PVDF (with a ratio of 8:2 wt/wt) on Celgard 2500, followed by drying at 50 ℃ under vacuum for 12 h.

The hSCNC layer on the Celgard 2500 membrane is ~15 µm in thickness with a loading of ~0.4 mg cm^{-2}.

Table S3. Li-S battery performances of S-doped carbons in this study and literatures.

Materials	Sulfur content (wt%)	Sulfur loading (mg cm^{-2})	Interlayer loading (mg cm^{-2})	Current density (A g^{-1})	Cycles	Retained capacity (mAh g^{-1})	Decay rate %	Max rate capacity (mAh g^{-1}/A g^{-1})	Max areal capacity (mAh cm^{-2}/A g^{-1})	Ref.
hierarchical S-doped carbon nanocages	77.4	1.1	0	2	400	579	0.07	686/2	1.2/0.2	This work
		4.5	0.4	0.1	80	959	0.20	632/1	4.7/0.1	
S-doped ordered mesoporous carbons	42	0.38	0	0.17	50	857	0.20	55/1.67	0.34/0.08	9
S-doped ordered mesoporous carbons	70	N/A[b]	0	0.17	100	200	0.60	N/A	N/A	10
hierarchical S-doped carbon aerogel	80	N/A	0	1.67	400	590	0.07	N/A	N/A	11
S-doped mesoporous graphene microspheres	60	N/A	0	8.4	140	710	0.13	830/13.4	N/A	12
3D S-doped graphene	80	2.5	0	0.84	350	785	0.08	590/3.35	3.0/0.33	13
		5.1		0.84	100	710	0.22	N/A	4.1/0.84	
S-doped microporous carbon interlayer	60 (e)[a]	1.5	3.7-4.3	3.35	500	720	0.06	781/8.4	2.28/0.33	14
		2.5		1.67	250	738	0.07	N/A	2.23/1.67	

Notes: (a) Sulfur content in the electrode. (b) Not available.

REFERENCES

1. L. Wang, R. Feng, J. Xia, S. Chen, Q. Wu, L. Yang, X. Wang and Z. Hu, *Acta Chim. Sinica*, 2014, **72**, 1070-1074.
2. K. Xie, X. Qin, X. Wang, Y. Wang, H. Tao, Q. Wu, L. Yang and Z. Hu, *Adv. Mater.*, 2012, **24**, 347-352.
3. L. Du, Q. Wu, L. Yang, X. Wang, R. Che, Z. Lyu, W. Chen, X. Wang and Z. Hu, *Nano Energy*, 2019, **57**, 34-40.
4. B. Delley, *J. Chem. Phys.*, 1990, **92**, 508-517.
5. B. Delley, *J. Chem. Phys.*, 2000, **113**, 7756-7764.
6. J. P. Perdew, K. Burke and M. Ernzerhof, *Phys. Rev. Lett.*, 1996, **77**, 3865-3868.
7. W. S. V. Lee, M. Leng, M. Li, X. L. Huang and J. M. Xue, *Nano Energy*, 2015, **12**, 250-257.
8. J. Heeg, C. Kramer, M. Wolter, S. Michaelis, W. Plieth and W. J. Fischer, *Appl. Surf. Sci.*, 2001, **180**, 36-41.
9. F. Nitze, K. Fossum, S. Xiong, A. Matic and A. E. C. Palmqvist, *J. Power Sources*, 2016, **317**, 112-119.
10. K. A. See, Y. S. Jun, J. A. Gerbec, J. K. Sprafke, F. Wudl, G. D. Stucky and R. Seshadri, *ACS Appl. Mater. Interfaces*, 2014, **6**, 10908-10916.
11. D. Li, G. Chang, L. Zong, P. Xue, Y. Wang, Y. Xia, C. Lai and D. Yang, *Energy Storage Mater.*, 2019, **17**, 22-30.
12. X. Ma, G. Ning, Y. Wang, X. Song, Z. Xiao, L. Hou, W. Yang, J. Gao and Y. Li, *Electrochim. Acta*, 2018, **269**, 83-92.
13. N. Li, F. Gan, P. Wang, K. Chen, S. Chen and X. He, *J. Alloy. Compd.*, 2018, **754**, 64-71.
14. J. Yang, F. Chen, C. Li, T. Bai, B. Long and X. Zhou, *J. Mater. Chem. A*, 2016, **4**, 14324-14333.